Blind restoration of turbulence degraded images based on two-channel alternating minimization algorithm*

YANG Huizhen[1,2], LI Songheng[1], LI Xin[1], ZHANG Zhiguang[1,2], YANG Haibo[3], and LIU Jinlong[1,2]**

1. Jiangsu Ocean University, Lianyungang 222005, China

2. Jiangsu Marine Resources Development Research Institute, Lianyungang 222005, China

3. Key Laboratory of Electro-Optical Information Control and Security Technology, The 53th Research Institute of China Electronic Technology Group Corporation, Tianjin 300308, China

(Received 21 August 2021; Revised 7 November 2021)

Due to the atmospheric turbulence and the system noise, images are blurred in the astronomical or space object detection. Wavefront aberrations and system noise make the capability of detecting objects decrease greatly. A two-channel image restoration method based on alternating minimization is proposed to restore the turbulence degraded images. The images at different times are regarded as separate channels, then the object and the point spread function (PSF) are reconstructed in an alternative way. There are two optimization parameters in the algorithm: the object and the PSF. Each optimization step is transformed into a constraint problem by variable splitting and processed by the augmented Lagrangian method. The results of simulation and actual experiment verify that the two-channel image restoration method can always converge rapidly within five iterations, and values of normalized root mean square error (*NRMSE*) remain below 3% after five iterations. Standard deviation data show that optimized alternating minimization (OAM) has strong stability and adaptability to different turbulent levels and noise levels. Restored images are approximate to the ideal imaging by visual assessment, even though atmospheric turbulence and systemnoise have a strong impact on imaging. Additionally, the method can remove noise effectively during the process of image restoration.

Document code: A **Article ID:** 1673-1905(2022)02-0122-7

DOI https://doi.org/10.1007/s11801-022-1128-4

The imaging of astronomical or space objects is always interfered by atmospheric turbulence and system noise, so the images of them are blurred[1]. Wavefront aberrations and detector noise make image quality decrease considerably. To meet the requirements for precise spatial positioning and object recognition, it is necessary to restore the images utilizing different image processing methods.

The imaging process can be regarded as a convolution operation between the point spread function (PSF) and the object. At the same time, the imaging process also introduces noise due to the limitation of detector performance. Then the image restoration is the process of deconvolution and denoising. Speckle imaging[2], lucky imaging[3], and phase diversity (PD)[4] have been successfully applied to restore astronomical or space objects. Speckle imaging needs a reference object and thousands of short-exposure images. The restoration accuracy of the lucky imaging depends on the probability of obtaining a "lucky image" and is only suitable for the situation that turbulence has a slight effect on the imaging[5]. Although the PD method can be used for the point sources and extended objects, it needs extremely complex calculation, and its convergence speed is very slow[6].

The blind deconvolution algorithm is widely used because of low system cost and no requirement of prior knowledge[7]. This kind of algorithm is often not stable enough and very sensitive to noise in the case of low photon levels. AYERS et al[8] used the non-negativity of the image as a prerequisite and proposed a single-channel iterative blind deconvolution method. Single-channel blind deconvolution presents long calculation time, inconsistent results, and non-convergence. Multi-frame blind deconvolution was submitted when multiple images of the same scene can be obtained[9,10]. SCHULZ first applied the method to process Hubble space telescope images. HIRSCH et al[11] presented a technique for multi-frame deconvolution called online blind deconvolution (OBD). KANAEV et al[12] have done a lot of research on eliminating noise in multi-frame blind deconvolution.

* This work has been supported by the National Natural Science Foundation of China (No.11573011), the Six Talent Peaks Project of Jiangsu Province (No.KTHY-058), the '333' Talent's Project in Jiangsu Province (No.BRA2019244), and the Research and Practice Innovation for Postgraduate in Jiangsu Province (No.KYCX20_2961).

** E-mail: liujinlong@jou.edu.cn

Most multi-frame blind deconvolution methods use multiple images to estimate the PSF, and then restore the object by deconvolution. The disadvantage is that it cannot remove the noise effectively, which can easily lead to the ringing effect of the restoration result. Additionally, most of the restoration methods mentioned assume that the turbulence is frozen and use this as a prerequisite, whereas, the turbulence changes dynamically indeed. Based on the alternating minimization algorithm[13], a two-channel image restoration algorithm is proposed in this paper. In this method, two images at different times are regarded as two channels, and then the object and its PSF are estimated alternately.

Assuming that there are P images (P>1) corresponding to the unknown object u, the mathematical optical imaging model can be written as

$$g_k = h_k * u + n_k, (1 \le k \le P), \tag{1}$$

where g_k is the image, h_k denotes PSF, and n_k is noise in the kth observation. The operator * stands for convolution. Estimating an unknown object u from g_k is ill-posed. This problem can only be solved by regularization, and its solution can be described as

$$\min_{u,\{h_k\}} F(u,\{h_k\}) + Q(u) + R(\{h_k\}), \tag{2}$$

where F is the data fidelity term, Q is the regularizer of the object, and R is the regularizer of PSFs. The function F is defined as

$$F(u,\{h_k\}) = \frac{\gamma}{2}\sum_{k=1}^{K}\left\| u * h_k - g_k \right\|^2, \tag{3}$$

where γ is the weight of the fidelity term, and $\|\bullet\|$ is the L_2 norm. Alternating minimization is used to solve Eq.(2). This problem is split into two sub-problems:

$$u\text{-step}: \min_u F(u,\{h_k\}) + Q(u), \tag{4}$$

and

$$h\text{-step}: \min_{\{h_k\}} F(u,\{h_k\}) + R(h_k). \tag{5}$$

Convergence to the global minimum is not guaranteed theoretically since the unknown variables are coupled in F. However, each sub-problem converges to its global minimum separately, and it can be solved by the augmented Lagrangian method efficiently. In general, the global minimum of Eq.(2) is attainable after a few alternations between the sub-problems. This method achieves image restoration by optimizing the u-step and h-step alternately. Augmented Lagrangian and total variation methods are used to promote the convergence of the solution for the object, and the Laplacian operator is used to enhance the robustness against noise for PSF.

Based on above-mentioned alternate minimization algorithm, a two-channel image restoration method is presented in this paper, which regards different images at different times as multiple channels and then estimates the object and PSF alternately. The initial alternating minimization in Ref.[13] is suitable for motion blur. Compared with motion blur, the aberration caused by dynamic atmospheric turbulence is more diffuse and complicated. The initial alternating minimization is applied to restore the turbulence degraded images, which needs to optimize the object and PSF continuously, and we call it optimized alternating minimization (OAM).

The multi-scale approach can describe the features of PSF from different scales. A big-scale can improve the accuracy of estimated PSFs, but it results in a long computational time. On the other hand, the too small scale cannot meet the performance requirements of restoration. For motion blur, it is reasonable to ensure the accuracy that the scale is set at 2. To compromise the accuracy and computational time, the scale should be selected at a relatively high value in image restoration. The weight of the fidelity term γ guarantees the solution to be consistent with the degradation process. PSF will become blurred and is prone to noise for a large γ. Estimated PSFs will focus only on small areas with a low γ. To obtain accurate PSF, γ should be adjusted as an appropriate value between 10^{-3} and 10^{-5} in image restoration. Due to the complexity of atmospheric turbulence, the number of iterations is more than that of motion blur theoretically. Each iteration includes an h-step and a u-step. In our experiment, the scale is set to 3, γ is adjusted as 10^{-4}, and the iteration is 15.

In astronomical or space object detection, the object is blurred by atmospheric turbulence and detector noise. The main noise contribution comes from photon noise, background noise, readout noise of the imaging sensor and dark current noise. In general, background noise follows a Poisson distribution with the mean and variance both as N_b. Readout noise follows a Gaussian distribution with zero mean and variance σ_r^2. Dark current noise can be regarded as a constant N_d. When the number of background noise photons is greater than 10, the system noise can be approximated as a Gaussian random distribution with mean N_B=N_d+N_b and variance $\sigma_B^2 = \sigma_r^2 + N_b$ [14]. In the subsequent experiment, we use the above mathematical model to simulate noise. Then images with different degrees of noise can be obtained by adjusting the value of N_d, N_b and σ_r^2. To quantify the amount of image noise, we define the following signal-to-noise ratio (*SNR*)

$$SNR = 10\log_{10}\frac{Var(u)}{Var(g - h * u)}, \tag{6}$$

where $Var(u)$ denotes the variance of the pixel values of u.

Root mean square error (*RMSE*) is used to evaluate the restoration performance[15]. Supposing two $m\times n$ monochrome images I and K, *RMSE* is defined as

$$RMSE = \sqrt{\frac{1}{mn}\sum_{i=0}^{m-1}\sum_{j=0}^{n-1}\left\| I(i,j) - K(i,j) \right\|^2}, \tag{7}$$

where I is an ideal image and K is the reconstructed image. The smaller the *RMSE* value, the better the restoration performance. Experiments results are presented in normalized root mean square error (*NRMSE*) finally.

In subsequent experiments, the method proposed by RODDIER[16] is used to simulate atmospherically

distorted wavefronts. Phase screens are generated at different atmospheric turbulence levels. In theory, the smaller the atmospheric coherent length r_0, the stronger the turbulence, and the greater the influence on the imaging of astronomical or space objects. In practice, D/r_0 is usually used to describe the effect of atmospheric turbulence on imaging, where D is the aperture of the telescope. When D is determined, the smaller the value of the atmospheric coherence length r_0 is, the greater the influence degree is. It is generally considered in related research areas that D/r_0=20 represents relatively strong atmospheric turbulence, and D/r_0=5 stands for weak atmospheric turbulence. Distorted wavefronts are selected randomly as the blur kernels. The experiment is performed on a PC with a 3.30GHz Intel(R) Core(TM)i5-4590 CPU in the Matlab program environment.

The original object, called satellite, is given in Fig.1(a). The grayscale of the images is from 0 to 255, and the image size is 512×512 pixels. The diffraction limit angle (λ/D) is supposed to be 5 pixels. Then the entire field of view is about 102 times of the size of diffraction-limited angle. Fig.1(b) shows the perfect imaging. It is noted that the ideal imaging and original PSFs are unknown in practical applications.

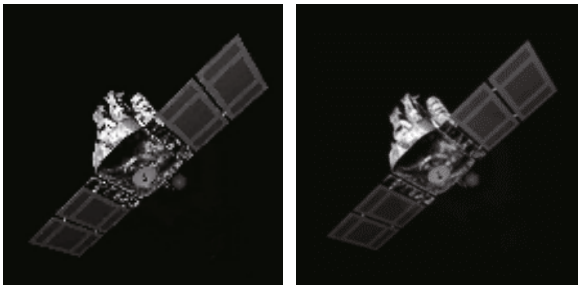

(a) (b)

Fig.1 (a) Original object-satellite image and (b) its corresponding perfect imaging effect

To investigate the convergence and robustness of OAM, corresponding PSFs of 200 different phase screens under one turbulent level are used as the blur kernels to obtain 200 different blurred images. All of these blurred images are divided into 100 groups randomly. The object image can be restored through one group (two blurred images) by OAM, and the average of 100 groups is considered as the ultimate experimental result. Image restoration results and convergence and stability of OAM are examined under different noise levels when D/r_0 are 5, 10, 15, 20 and 25, respectively. For comparison, the OBD proposed by HIRSCH[11] is also investigated.

The average convergence of *NRMSE* for different noise levels and different turbulent strengths are shown in Fig.2. From Fig.2, one can see that OAM can converge rapidly under different turbulent strength and different noise levels. The iteration needed for convergence is about five times under different conditions. Values of *NRMSE* remain below 3% after five iterations, and it does not increase with the growth of turbulence strength and noise level, which indicates that OAM has good robustness and adaptability to different turbulent strengths and different noise levels.

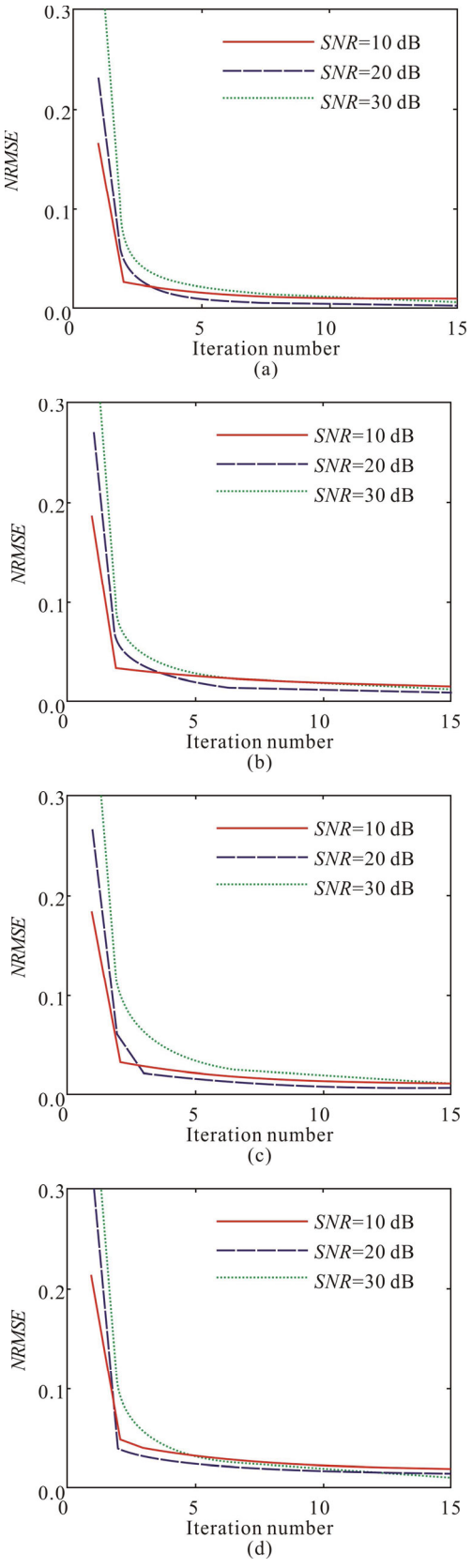

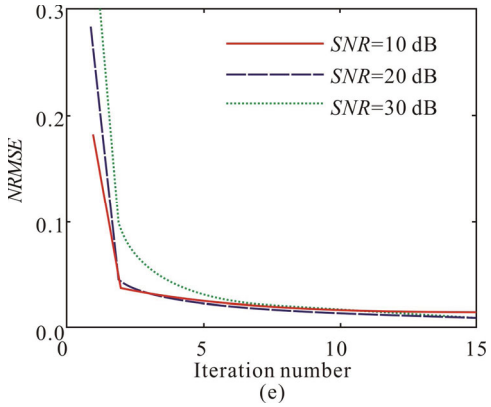

Fig.2 *NRMSE* curves under different turbulent strength and noise levels, where (a)—(e) are for D/r_0=5, 10, 15, 20 and 25, respectively

To further examine the stability and the adaptability of OAM, we use the standard deviation of *NRMSE* of 100 groups to analyze the dispersion degree from the average. Curves of the standard deviation under different turbulence levels and *SNR* are presented in Fig.3. Fig.3 shows that the standard deviation curves for D/r_0=5, 10, 15, 20 and 25 converge at 2‰ after about five iterations under three noise levels. Although the turbulence has a strong impact on imaging, when D/r_0 is set at 20 or 25, the values of standard deviation are slightly higher than that of D/r_0=10, and the values remain below 5‰. Additionally, all curves are close to zero after 10 iterations. The above data and tendency show that the proposed OAM has strong stability and adaptability.

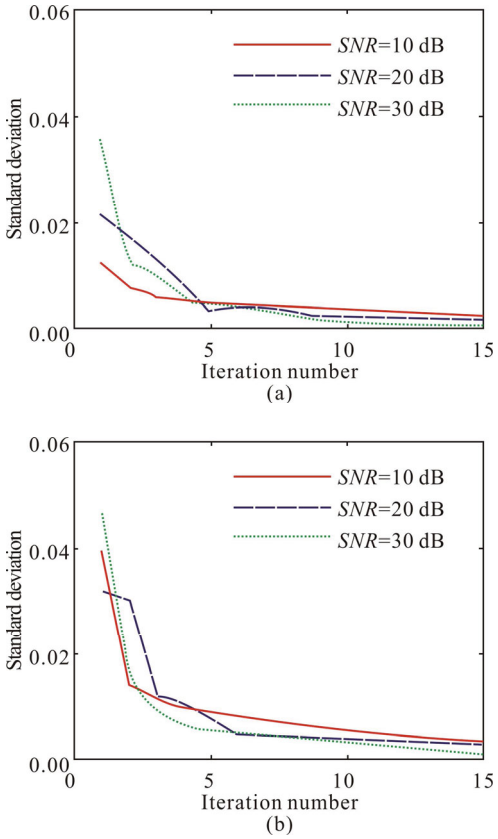

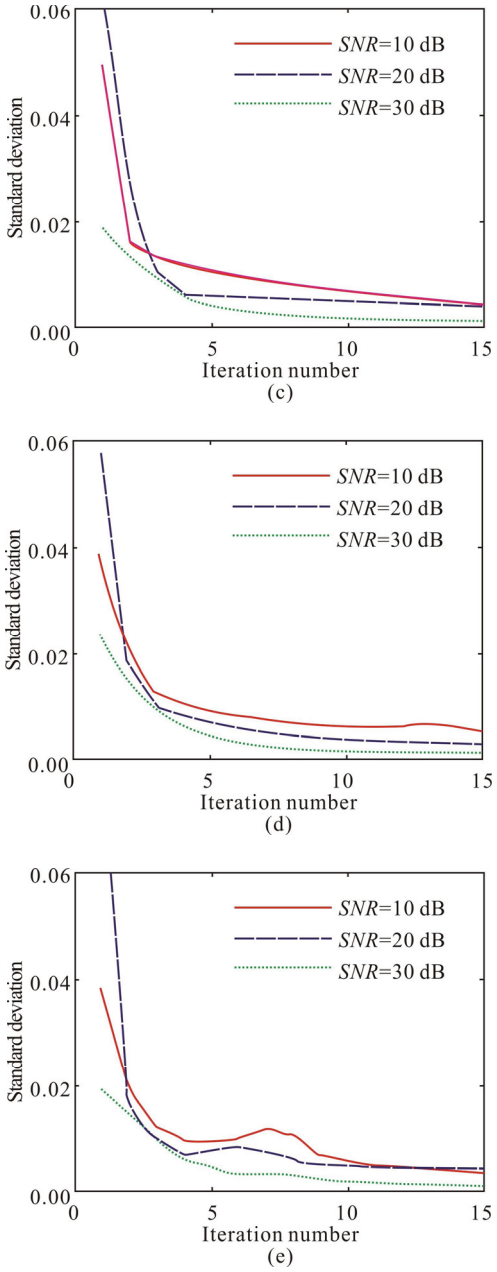

Fig.3 Standard deviation curves under different turbulent strength and noise levels, where (a)—(e) are for D/r_0=5, 10, 15, 20 and 25, respectively

To inspect the restoration effects, the corresponding images are shown in Fig.4 under the condition of D/r_0=20 with different noise levels. Two different PSFs, whose sizes are 64×64 pixels, are shown in Fig.4(a) and (c). Corresponding blurry images of satellite are illustrated in Fig.4(b) and (d), where the noise level *SNR* is 30 dB. Compared with the imaging in Fig.1(b), the blurry images in Fig.4(b) and (d) deteriorate severely, and it's almost impossible to distinguish the object.

Estimated PSFs from blurry images of satellite by OAM are presented in Fig.5(a) and (b). Fig.5(c) shows the recovery image. Compared with the imaging in Fig.1(b), Fig.5(c) is only slightly blurred in visual observation. In other words, Fig.5(c) is very close to the

ideal imaging.

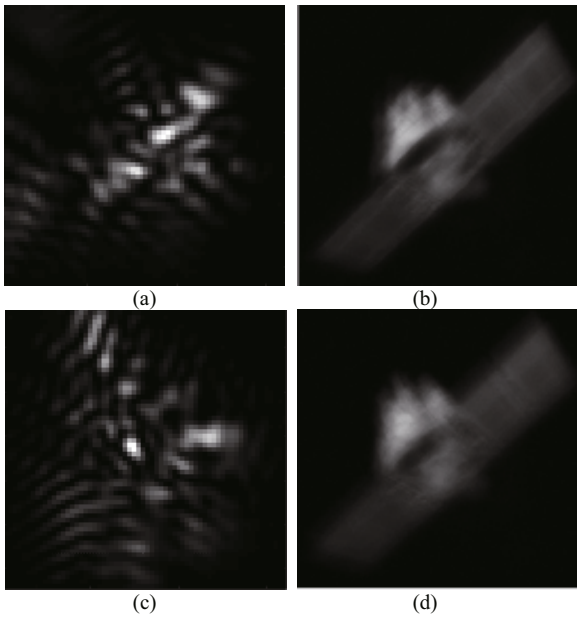

Fig.4 Original PSFs and blurry images at D/r_0=20 and *SNR*=30 dB: (a) PSF1; (b) Imaging A1 of satellite by PSF1; (c) PSF2; (d) Imaging A2 of satellite by PSF2

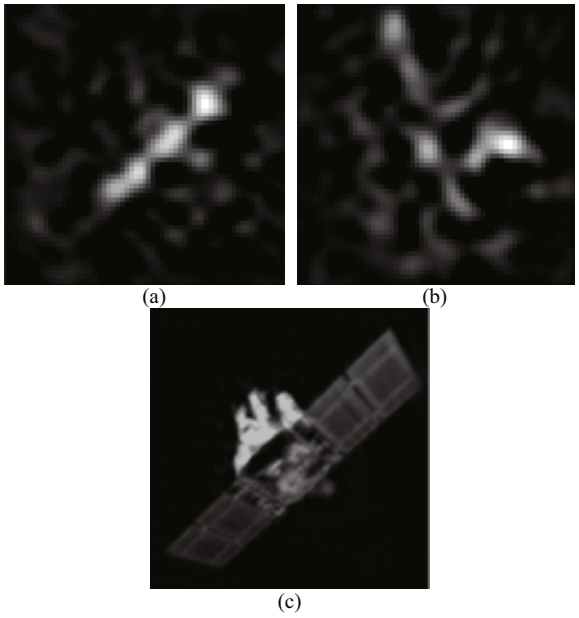

Fig.5 Recovery results at D/r_0=20 and *SNR*=30 dB: (a) Estimated PSF1 from A1; (b) Estimated PSF2 from A2; (c) Estimated image of satellite

Similarly, experiments are implemented at D/r_0=20 under high noise level, and results are given in Fig.6 and Fig.7, where the *SNR* is set at 20 dB and 10 dB, respectively. Fig.6(a) and (b) are two blurry images selected randomly, and Fig.6(c) and (d) are the restored images by OAM and OBD, respectively. For OBD, we simulate 30 frames of blurry images to obtain the results. Compared with restored images in Fig.6(c) by OBD, images in Fig.6(b) are sharper, and the quality is comparable to the ideal imaging by visual assessment. And Fig.7 can get the same comparison result. Additionally, OAM algorithm can remove noise effectively during the process of image restoration and preserve more image details.

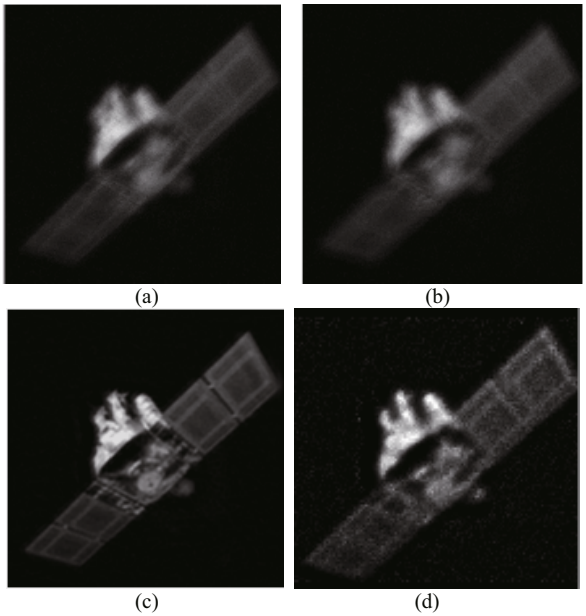

Fig.6 Blurry and reconstructed images of satellite at D/r_0=20 and *SNR*=20 dB: (a), (b) Two blurry images selected randomly; (c) Image reconstructed by OAM; (d) Image reconstructed by OBD

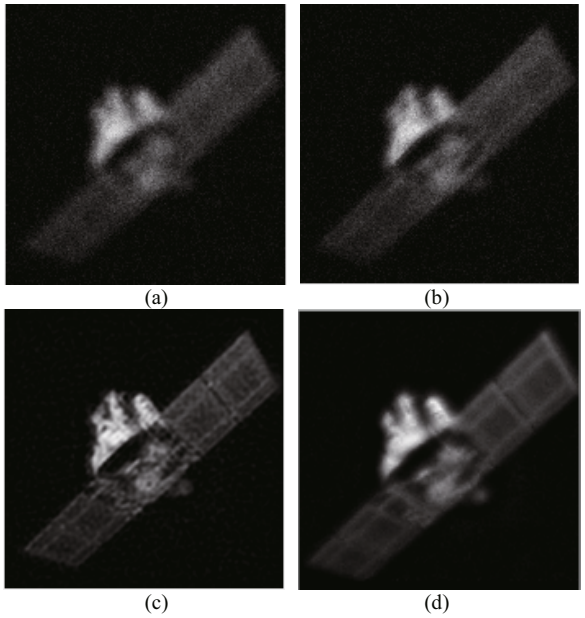

Fig.7 Blurry and reconstructed images of satellite at D/r_0=20 and *SNR*=10 dB: (a), (b) Two blurry images selected randomly; (c) Image reconstructed by OAM; (d) Image reconstructed by OBD

As seen from the above discussion, OAM can efficiently restore the images suffered from atmospheric

turbulence and system noise by simulation. To test and verify the algorithm performance well, an actual experiment is executed. In this experiment, a piece of stripe board is set as a space object and placed 2.4 km away from the observation telescope with an aperture of 1.3 m. Fig.8(a) is the original object of the stripe board with basic structural features. Fig.8(b) and (c) are two blurred pictures selected randomly from two hundred photos captured by charge coupled device (CCD), which are affected by turbulence and noise unknown. Fig.8(d) is the final reconstructed image by OAM. By visual observation, one can see that the definition of Fig.8(d) is far better than that of Fig.8(b) or (c). Meanwhile, quantitative assessment of image quality can be realized by mean opinion scores (*MOS*)[17], which is a method based on the fact that a high-contrast image is often more similar to its contrast enhanced image. The higher the *MOS*, the better the image quality. By calculation, the *MOS* of Fig.8(d) is 2.222 2 larger than those of Fig.8(b) and (c), which are 2.048 0 and 2.099 3, respectively. Thus, it can be seen that the actual experiment also fully validates the OAM has strong stability and adaptability.

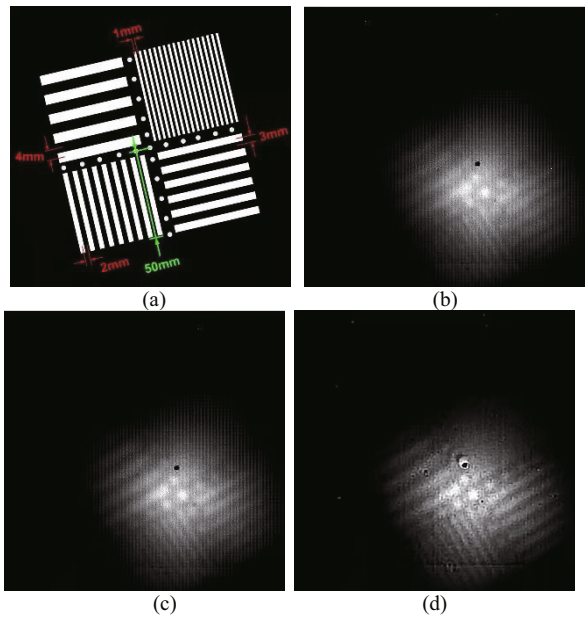

Fig.8 Experiments of stripe board: (a) Original object; (b), (c) Two blurred pictures selected randomly; (d) Image reconstructed by OAM

Due to the atmospheric turbulence and the system noise, the images are blurred in the astronomical or space object detection. It is necessary to restore the images by using different image processing methods. Based on the alternating minimization, we propose an imaging restoration method OAM, which is applicable for turbulence degraded images.

Collectively, simulation and actual experiment results verify that the proposed two-channel blind deconvolution based on alternating minimization can restore image well under different turbulence and noise levels. By statistical assessment, regardless of the turbulence strength and noise level, OAM can always converge rapidly within five iterations, and values of *NRMSE* remain below 3% after five iterations. Standard deviation data show that OAM has strong stability and adaptability to different turbulent levels and noise levels. Additionally, we compare the restoration results of the OAM with the well-known OBD method. OAM shows much better image quality and denoising capability than OBD. Additionally, the method we proposed can remove noise effectively during image restoration and preserve more image details. The above results can provide a promising approach for image restoration under strong turbulence and high noise levels in real applications.

Statements and Declarations

The authors declare that there are no conflicts of interest related to this article.

References

[1] RAO C H, TIAN Y, BAO H. AO-based high resolution image post-processing[M]//TYSON R K. Topics in adaptive optics, IntechOpen. Croatia：Intech, 2011：69-94.

[2] PARK J, CHOE Y, YEOM D I. A study on spatial filtering of a speckle image reflected from a scattering medium in a coherent beam combining system[J]. Journal of the Korean physical society, 2021, 78(8)：657-661.

[3] MACKAY C, RAFAEL R L, BRUNO F C, et al. AOLI—adaptive optics lucky imager：diffraction limited imaging in the visible on large ground-based telescopes[EB/OL]. (2012-07-17)[2021-06-30]. https：//arxiv.org/abs/1207.4065/.

[4] KE X Z, CUI N M. Experimental research on phase diversity method for correcting vortex beam distortion wavefront[J]. Applied physics B, 2020, 126(4)：1-11.

[5] MINARDI S, HARRIS R J, LABADIE L. Astrophotonics： astronomy and modern optics[J]. Astronomy and astrophysics review, 2021, 29(1)：1-84.

[6] XIANG Y Y, LIU Z, JINZ Y. High resolution solar image reconstruction method[J]. Progress in astronomy, 2016, 34(1)：94-110. (in Chinese)

[7] LIU T, YIN T T, GUO Y N. Research on single-channel blind deconvolution algorithm of single mixed image[C]//Proceedings of the 2021 Future of Information and Communication Conference (FICC), April 29-30, 2021, Vancouver, Canada. Cham：Springer International Publishing, 2021, 2：860-870.

[8] AYERS G R, DAINTY J C. Iterative blind deconvolution method and its applications[J]. Optics letters, 1988, 13(7)：547.

[9] CHEN L, YAP K H, HE Y. Efficient recursive multichannel blind image restoration[J]. EURASIP journal on advances in signal processing, 2007, 2007(1)：1-10.

[10] HAJMOHAMMADI S, NOOSHABADI S, ARCHER

G E, et al. Parallel hybrid bispectrum-multi-frame blind deconvolution image reconstruction technique[J]. Journal of realtime image processing, 2019, 16(7)：919-929.

[11] HIRSCH M, HARMELING S, SRA S, et al. Online-multi-frame blind deconvolution with super-resolution and saturation correction[J]. Astronomy and astrophysics, 2011, 531(Pt.2)：A9.

[12] KANAEV A, MILLER C W. Confidence measures of optical flow for multi-frame image reconstruction[C]//SPIE Defense, Security, and Sensing, April 23-27, 2012, Baltimore, Maryland, United States. Washington：SPIE, 2012, 8399： 23-34.

[13] SROUBEK F, MILANFAR P. Robust multichannel blind deconvolution via fast alternating minimization[J]. IEEE transactions on image processing, 2012, 21(4)：1687-1700.

[14] LIU J L, YANG H Z, LI X, et al. Error analysis and threshold selection in model-based wavefront sensorless adaptive optics system[J]. Optoelectronics letters, 2020, 16(5)：0327-0332.

[15] LI W, HE Y, WANG J, et al. Quality improvement of adaptive optics retinal images using conditional adversarial networks[J]. Biomedical optics express, 2020, 11(2)：831-849.

[16] RODDIER N A. Atmospheric wavefront simulation using Zernike polynomials[J]. Optical engineering, 1990, 29(10)：1174-1180.

[17] YAN J, LI J, FU X. No-reference quality assessment of contrast-distorted images using contrast enhancement[EB/OL]. (2019-04-18)[2021-06-30]. https：//arxiv.org/abs/1904.08879/.